Proceedings World Geothermal Congress 2020+1
Reykjavik, Iceland, April - October 2021

Forecasting Induced Seismicity and Maximizing Production of Electricity in EGS

Dimitrios Karvounis, and Stefan Wiemer

Swiss Seismological Service, ETH-Zurich, NO H 62, Sonneggstrasse 5, 8092, Zurich, Switzerland

karvounis@sed.ethz.ch

Keywords: Induced Seismicity, Probabilistic forecasting, Numerical Modeling, Optimization

ABSTRACT

Enhanced Geothermal Systems (EGS) has been for decades considered to be one of the best candidate technologies for exploiting the abundant geothermal energy stored in non-volcanic regions and their further development is now eminently needed for decarbonizing our society. Induced seismicity due to the stimulation of EGS reservoirs has been a major setback for the development of the technology since investors need not only to consider the risk of drilling an underperforming well, but also the seismic hazard and its social aspects. The governmentality of EGS is further restricted by the limited experience from successful EGS stimulations, the large number of possible scenarios that need to be considered, and by the complexity of the analytical models that best describe the physical processes during stimulation. Here, a Discrete Fracture Hybrid Model (DFHM) is employed for numerical studies, which DFHM combines deterministic numerical modeling of flow inside discrete fractures with stochastic modeling of seismicity. Given a stimulation strategy for the wells of an EGS, the DFHM returns in time for real-time applications both forecasts of induced seismicity that are useful for Probabilistic Seismic Hazard Assessments (PSHA) and forecasts of the maximum expected electrical power generation that is useful for Probabilistic Reservoir Performance Assessments (PRPA). Inference, prediction, probabilistic optimization, and uncertainty quantification can be performed with the DFHM for several scenarios related to induced seismicity in unconventional fractured reservoirs, for which scenarios conventional PSHA approaches fail due to their simplifications. The concept of multi-staged soft stimulation is tested with the DFHM, where both PSHA and PRPA are performed and compared with past single-staged strategies.

1. INTRODUCTION

Enhanced Geothermal Systems (EGS) is an unconventional geothermal technology that has the potential of matching the installed capacity of geothermal power plants within a few decades (Bertani, 2016). EGS can become part of the exclusive club of energy technologies that provide base-load energy for electricity and heating robustly and without being limited to volcanic countries. It is no surprise that EGS technology is an essential element of the future energy plans of several countries reported to Bertani (2016). In Switzerland, EGS technology is expected to provide up to 7% of electricity by the year 2050 and tens of EGS power plants are expected (Hirschberg et al., 2015).

Successful stimulations of the EGS reservoirs are necessary for the technology to reach its full potential. The EGS wells are drilled to depths of 2 - 8 km, and target hot enough pre-existing networks of fractures. The permeability of these fractures is too low for commercial exploitation and stimulation is required. During stimulation, cold pressurized water is injected to the network and reduces the frictional strength of the fractures until enough induced seismicity events due to hydro-shearing occur. In principle, the permeability of fractures that hydro-shear increases significantly and in a rather permanent manner. Once all wells have been successfully stimulated, then the EGS power plant can operate and generate electricity by circulating fluid through the enhanced fracture network. Cold water is injected through the injection(s) wells, the injected water extracts some of the heat stored in the EGS reservoir and it is eventually produced by the production well(s). Electricity and heat can then be co-generated. EGS power plants need to generate large amounts of electricity for decades in order to be financially self-sustainable. That would need the slipped fractures during stimulation to form an extensive interconnected cluster, within which flow is distributed rather uniformly; i.e. no dominant flow paths exist that can reduce produced temperature quickly and cause an early stopping of EGS production. Designing stimulation strategies with high chances of returning profits to the EGS investments is an open challenge for EGS, but it is not the main challenge.

The main challenge for EGS is the management of the induced seismicity risk. Past expensive EGS projects were unsuccessful due to damaging injection-induced earthquakes and their wells had to be abandoned. The most recent case is the EGS project in Pohang, South Korea that was canceled after the M_w 5.5 earthquake that followed its stimulation (Grigoli et al., 2018), which is the most damaging earthquake associated with EGS since it injured more than 100 people and financial losses because of it are expected to reach $300 million (Lee et al., 2019). Ideally, the fracture network in EGS should be enhanced only with benign seismic events, but managing induced seismicity risk is a challenge for several technologies and not only for EGS. Foulger et al., (2017) reviewed human-induced earthquakes from several technologies concluding that geothermal operations, water reservoirs, and conventional oil and gas exploitation face the highest hazard.

The maximum magnitude observed in sequences of induced seismicity remains statistically as frequent as the Gutenberg-Richter law would expect (van der Elst, 2016). This finding implies that the possibility of triggering an event with undesired magnitude during EGS stimulation can be limited by reducing the number of events required for enhancing the EGS. Moreover, findings from underground experiments imply that the repeatability of a certain strategy is doubtful since implementing the same strategy twice can give different number of events even within the same reservoir (Amann, 2018). Governing the induced seismicity risk should be tailor-made for each site and up-to-date with the most recent observations (Lee et al., 2019). Probabilistic Seismic Hazard Assessments (PSHA) performed in real time can assist in governing the induced seismicity risk.

Up until now, the majority of the relatively few EGS-related stimulations have been safely concluded (Lu, 2018) and many stimulation strategies have been tested but conclusive generic evidence were reached neither for their safety nor for the commercial interest of their enhanced reservoirs. Step rate injection at the casing shoe of the well was the stimulation strategy at both the EGS in Basel, Switzerland and in Soultz-sous-Forêts, France, but alarming earthquakes were triggered only in Basel (Evans et al., 2005; Häring et al., 2008). Since then, new promising strategies have been suggested including the cyclic soft stimulation that was one of the several different stimulation strategies injected in Pohang (Hofmann et al., 2019) and the multi-staged concept recently performed near Helsinki, Finland (Kwiatek et al., 2019), where segments of the well are isolated and stimulated separately. Out of these projects, only the EGS in Soultz-sous-Forêts has been operated over a long time. Given the necessity of limiting the number of earthquakes, real-time Probabilistic Reservoir Performance Assessments (PRPA) could predict the least number of events still required for an EGS reservoir with optimal properties. These forecasts should ideally be consistent with the performed PSHA as it could make continuing planned injections obsolete.

Risk-based traffic light systems that operate in real-time during injection are the state-of-the-art in managing induced seismicity. After the M_w 5.5 earthquake at the EGS in Pohang, where no risk-based traffic light was employed, making risk-based decisions is strongly recommended for future EGS stimulation (Lee et al., 2019). Such an Adaptive Traffic Light System (ATLS) is being developed by the Swiss Seismological Service (SED), it will be employed in future EGS stimulations (Karvounis et al., 2014, Mignan et al., 2017), and it is based in probabilistically forecasting induced seismicity. It takes into consideration the building stock to which the EGS is exposed to, as well as all field observations collected prior to stimulation such as borehole measurements and hydraulic well tests. Then, during the stimulation and in real time, it recalibrates several forecasting models, collects all new forecasts, combines them to a single new forecast and returns its probabilistic forecast for the induced seismicity risk (Kiraly et al., 2016). The step of forecasting induced seismicity is essential, since without it Probabilistic Seismic Hazard Assessments (PSHA) are not possible. Goal of ATLS is to return forecasts for excessive induced seismicity risk in time for the operators to take measures and to mitigate this risk.

Here, results from our three-dimensional hybrid model that employs discrete modeling for fractures and is highly adaptive to dynamically changing fracture networks because of seismicity is presented. This Discrete Fracture Hybrid Model (DFHM) was presented in more detail by Karvounis et al. (2014) and by Karvounis and Wiemer (2015). Here it is discussed how its implementation has been accelerated for the needs of a real-time traffic light, and how it can be employed for designing stimulation strategies that optimally exploit the induced seismicity events.

2. DISCRETE FRACTURE HYBRID MODEL

2.1 Governing Equations for Deterministic Flow and Heat Transport Modeling

Single phase laminar flow of an incompressible fluid is considered everywhere inside the three-dimensional domain of the EGS reservoir $\Omega \epsilon \boldsymbol{R}^3$. Mass conservation at time moment t is expressed inside Ω as

$$S\frac{\partial p}{\partial t} = \nabla \cdot \left(\frac{\mathbf{K}}{\mu} \cdot \left(\nabla p - \rho \mathbf{g} \nabla z \right) \right) + q + Q \,, \tag{1}$$

where $S, p, \boldsymbol{K}, \mu, \rho, \boldsymbol{g}, z, q, Q$ are compressibility, pressure, the tensor of permeability that is anisotropic along fractures, fluid viscosity, fluid density, vector of gravitational acceleration, depth, the stimulation strategy and the rest of the natural sink/source terms. The term inside the parenthesis in eq. (1) is the opposite of the Darcy's fluid velocity u. Without loss of generality, an impermeable medium (e.g. granite) is considered for which it is assumed that porosity equals $\boldsymbol{K} = 0$ and flow is possible only within the void volume inside fractures.

Besides density, specific heat capacity c_v is also considered steady and energy conservation inside Ω is modeled as

$$c_v \rho \frac{\partial T}{\partial t} + \nabla \cdot \left(c_v \rho T \mathbf{u} \right) = \nabla \cdot \left(\mathbf{\Lambda} \cdot \nabla \mathrm{T} \right) + w + W \,, \tag{2}$$

where $T, \boldsymbol{\Lambda}, w, W$ are the temperature, the tensor of heat conductivity, heat source/sink from the wells, and the rest of heat sources. Two materials are considered in eq. (2). Inside fractures the fluid's properties are considered and everywhere else, the material properties of the impermeable hot medium that surround the fractures. Inside fractures, advection is the dominating mechanism of heat transfer and therefore $\boldsymbol{\Lambda} \rightarrow 0$. Inside the impermeable matrix heat is transferred only by conduction since $\boldsymbol{u} = 0$.

The total electrical energy E generated by converting to electricity the produced heat and over a period of time t_l equals

$$E = -\int_0^{t_l} \eta_{el} \left(\int_\Omega w d\Omega \right) dt \approx \int_0^{t_l} \eta_{el} F_p \rho c_v \left(T_p - T_i \right) dt \,, \tag{3}$$

where η_{el}, F_p, T_p, T_i are the efficiency with which heat is converted to electricity, the produced rate, the produced temperature and the injection temperature. The efficiency of the Carnot cycle is a physical upper limit for η_{el} and it decreases with decreasing produced temperature. For the range of thermodynamic conditions at which EGS plants operate, the analytical model η_{el} suggested by Zarrouk and Moon (2014)

$$\eta_{el} = 0.078795 \cdot \log\left(h_p \right) - 1.00081 \,, \tag{4}$$

is a good fit to the current status of conversion efficiencies, where h_p is the produced enthalpy of the fluid in kJ/kg.

2.2 Governing Equations for Stochastic Modeling of Induced Seismicity

In contrast to flow and heat transport, no deterministic mechanical modeling is considered here. A three-dimensional seed-model is employed for this purpose that samples several seeds and their properties. Each seed represents a fracture patch that can be reactivated seismically when pre-defined scenarios are simulated. For simplicity, a disk-shape patches are assumed for all the seeds and the properties of the seeds are steady during simulations. These properties for the m-th sampled seed (or patch) are $\{\boldsymbol{X}_s, M_w, R_s, \boldsymbol{n}_s, \Delta\tau, C_0, \mu_s, \boldsymbol{\sigma}_1, \boldsymbol{\sigma}_2, \boldsymbol{\sigma}_3\}^m$ and represent the hypocenter, the moment magnitude of the expected earthquake, the radius of the disk-shaped slipped surface, the pole vector of the plane, the stress drop of the event, the cohesion of the fracture, the fracture's friction, and the initial three principal stress vectors, respectively.

The Mohr-Coulomb failure criterion is the cornerstone of the pre-defined geo-mechanical scenario considered here. According to the criterion, an induced seismicity event with hypocenter X_s and source time t_s occurs only if the pressure there equals to

$$p(X_s, t_s) = P_f = \frac{C_0 - \tau}{\mu_s} + \sigma_n \,, \tag{5}$$

where P_f, σ_n, τ are the failure pressure at which the earthquake initiates, the normal compressive stress to the fracture's plane, and the shear stress on the fracture. An exponential distribution that resembles the Gutenberg-Richter law is considered for the frequency with which M_w are sampled among the seeds. The moment magnitude M_w of each event is sampled independently of the rest properties and with the cumulative density function

$$F(M_w) = 1 - 10^{-b(M_w - M_{w,min})} \,, \tag{6}$$

where b is the b-value of the resulting Gutenberg-Richter distribution, and $M_{w,min}$ is the minimum possible moment magnitude. By combining the relationship between moment magnitude and moment by Hanks and Kanamori (1979) and the relationship between moment and equivalent slip radius by Eshelby (1957), the effective radius size R_s of such a slip is

$$R_s = \sqrt[3]{\frac{7}{16\Delta\tau}} \cdot 10^{\frac{1}{2}(M_w + 6.03)} \,. \tag{7}$$

By considering Eqs. (5 - 7), the dimensions of the sampling space are reduced to the dimensions of the random variables $\{\boldsymbol{X}_s, M_w, \boldsymbol{n}_s, \Delta\tau, P_f\}^m$, where the total number of seeds m_{max} is also a variable. Field observations before and during the stimulation can reduce uncertainty for these variables. For example, uncertainty about P_f and $\boldsymbol{n}_s$ can be reduced with stress measurements and images of the well, and with observed seismicity and its focal mechanisms. Stress drop $\Delta\tau \approx$ 2-3 MPa is typically considered given to the low sensitivity of eq. (7) to it.

Irreducible prior to stimulation are the parameters $\boldsymbol{X}_s$ and M_w that need to be forecasted. For the sampling of magnitudes M_w, the expected b-value is considered since it allows forecasting induced seismicity probabilistically (van der Elst, 2016). For hypocenters, fractures are assumed to come in sets and each set has its density of seeds. Within a volume, seeds are assumed uniformly distributed and the total number of seeds sampled for that volume follows a Poisson distribution based on the density of each set. Source time ts is never treated as a random variable, but as deterministic since it needs to satisfy the solution of eq. (1).

2.3 Permeability Enhancement from Induced Seismicity

Induced seismicity in EGS seems unavoidable since the permeability of the pre-existing fractures inside the reservoir is too low to allow producing at commercial rates. This low permeability is captured by the low values of Equivalent Porous Media (EPM) permeability measured at an unstimulated EGS well k_0. Goal of the stimulation is to increase this EPM permeability by several orders of magnitude.

When the fluid pressure inside a fracture patch reaches P_f and the condition of eq. (5) is satisfied, then a seismic event due to hydro-shearing occurs and the two rough surfaces of the fracture slip relative to each other. Slipping lasts very shortly and eq. (1) is not representative enough for pressure changes during that short time. During slipping, neither p is continuous nor is the assumption of incompressible single phase representative enough. The new resting position of the two slipped fracture surfaces is such that the distance between the two plates that is called 'mechanical aperture' and it has increased from $b_{m,0}$ to $b_{m,1}$ in an almost irreversible manner. Typically it is expected $b_{m,0} < b_{m,1}$ and the same applies for the permeability of the patch that increases from $k_{f,0}$ to $k_{f,1}$. Hydraulic aperture is defined as the distance between two parallel plates that experiences the same pressure drop with flow as the fracture. This hydraulic aperture b_h needs to be considered for the cubic law

$$k_f = \frac{b_h^2}{12} \,. \tag{8}$$

Experiments by Lee and Cho (2002) showed that the ratio $b_h / b_m \approx 0.2$ can be realistic for EGS.

Fine effects happening during slipping are neglected here, and instantaneous changes for both b_h and b_m are assumed, while the compressibility S of the slipped fracture never changes. The mechanical aperture increases by δb_m and the fracture permeability increases to k_f, are represented in eq. (1) as instantaneous source terms Q and instantaneous step-wize increase of $\boldsymbol{K}$, respectively, that happen only along the thin disk of the slipped patch. In principle, real time well logs and seismic catalogs can reduce uncertainty about δb_m and k_f.

2.4 Real-time Probabilistic Assessments of Seismic Hazard and reservoir Performance with a Discrete Fracture Model

A Discrete Fracture Hybrid Model (DFHM) has been developed for forecasting two important phases in the lifetime of an EGS power plant when a stimulation strategy q is planned. The model combines deterministic and stochastic modeling. Analytical models (1) – (3) for flow and heat transport are numerically solved with the adaptive Hierarchical Fracture Representation (a-HFR) introduced by Karvounis and Jenny (2017) for EGS simulations and which method employs an embedded discrete fracture model. Stochastical models (5) – (7) are treated by the seed model presented by Karvounis et al., (2014) and Karvounis and Wiemer (2015).

The hybrid simulates first the 'creation phase', during which phase the wells are stimulated, injection-induced seismicity is highly probable and the EPM permeability enhances. Pressure is considered the unobserved hidden mechanism that reactivates fractures and potential slip patches in agreement with the observed field statistics are sampled by the seed model. Eq. (1) is numerically solved with an a-HFR model for every time-iteration, the source times t_s of the sampled seeds are found and then the a-HFR model is updated with an enhanced permeability tensor $\boldsymbol{K}$ and a new distribution for sources Q. The 'production phase' is the second phase simulated by the DFHM. Here, a-HFR is employed again and numerically solves Eqs. (1) – (3) for the enhanced permeability tensor $\boldsymbol{K}$. The production from the EGS wells and the total electrical energy production E can be estimated with a-HFR for any set of conditions at the EGS wells.

Benefits of employing a-HFR for simulating the creation and the production phase include the ability to discretize complex geometries with small grids and the ability of combining the benefits of discrete modeling for large and dominant fractures with the benefits of upscaling the rest of the fractures. Initially, a continuum with the EPM permeability k_0 is considered that represents the upscaled effect of the pre-existing fractures. This continuum is discretized with blocks of size $2 \cdot \Delta x$. Patches with $R < \Delta x$ are upscaled and the permeability of the continuum changes as explained by Karvounis and Wiemer (2015). This upscaling is based on numerical findings from studying the percolation threshold of three-dimensional circle-shaped fracture networks with power law distribution (Mourzenko et al., 2005). The compressibility of the upscaled continuum is the product of S and ρ_f, where ρ_f is the fracture density with units [m^{-1}]. Patches with $R \geq \Delta x$ are treated as discrete fractures with permeability k_f and compressibility S.

By the end of the creation phase's simulation, DFHM has found the N seeds with source times t_s within the simulated period and returns a synthetic catalog of induced seismicity with the source times and the sampled properties $\boldsymbol{H} = \{\boldsymbol{X}_s, M_w > M_{w,min}, \boldsymbol{n}_s\}^N$. Note, that with $\boldsymbol{n}_s$ and with the principal stresses for each event, the focal mechanism of each seed can also be found.

Of course, these synthetic catalogs are conditioned on the stimulation strategy q for every realization of the seed model. A Bayesian approach is employed for probabilistically forecasting induced seismicity $\boldsymbol{H}$ and electrical energy E for each q. M independent realizations of the seed model are simulated with the DFHM and M pairs of forecasts $U = \{\boldsymbol{H}, E\}$ are obtained. Mean values can be approximated with a Monte Carlo integration such that

$$\langle U \rangle \approx \frac{1}{M} \sum_{k=1}^{M} U^k , \tag{9}$$

where U^k represents the k-th forecast for the k-th realization of seeds, and the statistical error $\pm \delta U$ that is associated with the estimation of mean U equals

$$\delta U \approx \sqrt{\frac{1}{M-1} \left(\frac{1}{M} \sum_{k=1}^{M} \left(U^k\right)^2 - \langle U \rangle^2 \right)} . \tag{10}$$

Consistency is a necessary condition for comparing injection strategies with regards to expected revenue E and the same operational strategy for the wells needs to be considered. Here, the maximum possible revenue E^k for the enhanced permeability $\boldsymbol{K}^k$ are considered for the k-th realization of seeds. Maximization of E^k is achieved with the Brent algorithm, a line search optimization method that offered by the GSL library (Gough, 2009) and combines the golden ratio section method with a parabolic interpolation. Constraints considered for maximizing electricity E is that generation is possible only when $T_p > 100$°C, the conversion efficiency is given by eq. (4), and the bottom-hole pressure at the injection does not exceed $|\boldsymbol{\sigma}_3|$.

3. RETURNING FORECASTS IN NEAR REAL-TIME

Returning forecasts of induced seismicity and of E in near-real time is a necessary feature for integrating any forecasting method in ATLS since EGS operators need to be informed in time for taking risk mitigation measures or for finding alternative injections with higher expected E. The computational cost of the DFHM is dominated by the computational cost required for solving linear systems with N_x degrees of freedom (dof), by the number of simulated timesteps N_t, and by the efficiency with which the synthetic catalog is updated with every new solution for pressure p.

HFR-Sim is the in-house EGS simulator of ETH that solves flow and heat transport with a-HFR (Karvounis and Jenny, 2016) and it can also solve shearing for well-defined problems with the XFVM (Deb and Jenny, 2017). The implemented DFHM described below is based on a version of HFR-Sim, the coding of which is optimized by the Swiss National Supercomputing Center (CSCS) for the needs of ATLS. Besides code optimization, significant parts of HFR-Sim have been reprogrammed in C++11 and the Eigen library is employed for vector computations. Together with the methods presented here, a significant speed up in the forecasts has been achieved. Indicatively, the not optimized hybrid model presented by Karvounis and Wiemer (2014) required approx. 8 hours for forecasting a period of 2 weeks. The current version returns its forecast approx. 350 times faster and forecasts periods several times longer for the same problem. All Monte Carlo integrations are performed with direct sampling. Methods for accelerating the convergence of the Monte Carlo integration are not discussed here.

3.1 Linear System Solvers for the Discretized Governing Equations

HFR-Sim discretizes geological models by separating the domain Ω into many subdomains and then discretizes each subdomain independently of the rest. Each of the N_w well segments through which injection or production occurs are discretized with one 1D well cell of same length with the segment. Each of the slipped patches with $R \geq \Delta x$ or other dominant fractures are discretized with a 2D structured orthogonal grid. The rest of the slipped patches with $R < \Delta x$ and fractures that have not hydro-sheared are upscaled and represented by the 3D subdomain of 'damaged matrix' that is discretized with an equidistant orthogonal grid with grid-block of size $2 \cdot \Delta x$ and size N_r. Finally, one more subdomain is considered for solid hot rock that surrounds the fractures and inside which heat has been stored. Without loss of generality, the same $2 \cdot \Delta x$ grid of size N_r is employed for it. Once all subdomains are discretized, then the transmissibility is found that quantifies mass flow between cells of the same subdomain and cells of different subdomains. The well model implemented is the one suggested by Peaceman (Peaceman, 1978) and two point flux approximation is considered for the transmissibilites and the heat flux due to conduction.

The total number of dofs for modeling flow is $N_f \approx N_w + N_r + (A / \delta x_f^2)$, where A is the total discretized fracture surface. Note that the size N_f does not depend on the shape of A but mainly on its size. Similarly, the number of dofs for modeling heat is $N_h = N_r + N_f$.

HFR-Sim employs the linear system solvers from the Trilinos package. The partial differential eq. (1) is parabolic for $S > 0$, elliptic for $S = 0$, is solved implicitly for the N_f dofs, and its discretized problem is symmetric. The Algebraic MultiGrid (AMG) linear system solver is employed for this linear system. AMG solvers demonstrate a linear relationship between the computational cost required for converging to the solution and the size of the linear system N_f. Such optimum scaling of the computational cost with the size is not possible for the energy conservation eq. in (2) that is parabolic, but it is a diffusion-advection problem that is not symmetric. HFR-Sim solves the discretized energy equation of size N_h with a KLU direct solver, where a fixed step-size is considered so that only one completed LU factorization needs to be performed.

3.2 Adaptive implicit and step-size methods

The number of operations required by the AMG per linear system is proportional to the grid size N_f, which size increases with time as new patches slip and the size of discretized surface A increases. When the size of the simulation's time-step δt is fixed, then the overall simulated time is $\delta t \cdot N_t$. The number of operations required by AMG for simulating this time is going to be proportional to the products of N_t and the average N_f throughout the simulation.

Adaptive step-size methods returns solutions of comparable accuracy with fewer N_t iterations for the considered problem, by increasing the initial δt by a certain factor t_B with each iteration. The step-size for the k-th time-iteration is $\delta t \cdot (t_B)^{k-1}$. Also, the local error can be approximated for each iteration and the adaptive step-size solution can be further corrected by this error and to maintain accuracy comparable to the much finer δt.

A variation of the adaptive step-size method is implemented for the DFHM. Like in the original method, the time-step increases by the factor t_B with each iteration but it resets to δt when a new large patch with $R \geq \Delta x$ slips or when the boundary conditions change (e.g. new step-rate). Also, approximations of the local error are never performed, instead a maximum value is considered for the time-step that can never be exceeded. The accumulating error is bounded by the latter restriction. Practically, simulations with this adaptive step-size method are accelerated when the rate of seismicity is low. Low rates of seismicity are expected during post-injection periods.

Also for periods of low rates of seismicity where the adaptive step-size method is activated, a variation of the Adaptive Implicit Method (AIM) is activated too. AIM combine the advantages of implicit and explicit modeling by decomposing the computational domain to one domain that is solved implicitly and to one that is solved explicitly (Thomas and Thurnau, 1983). Explicit solutions require only one matrix-vector multiplication per time step for solving eq. (1), but an upper limit exists for the step-sizes that ensure stability. Implicit solutions from an AMG may require several matrix-vector multiplications until convergence but they are unconditionally stable, and conserve mass both locally and globally. AIM achieves the desired accuracy for least operations by appropriately decomposing the domain and treating implicitly fractures and other cells with too restrictive stability requirements.

The variation of the AIM implemented here, is customized to the needs of the DFHM. Instead of solving the original system of equations with size N_f, a smaller system of linear equations is created that can be solved implicitly with an AMG and its solution is close enough to the solution of the original problem. First, the computational grid is split into the N_r^{ex} cells that make sense solving explicitly and the $N_w + (A / \delta x_f^2) + N_r - N_r^{ex}$ cells that should be solved implicitly. The set of N_r^{ex} cells consists only of damaged matrix cells that are neither penetrated by a fracture, nor by a well, nor are expected to have been reached by the diffusing pressure front Δp by the next-iteration, where Δp is a user-defined parameter that controls the accuracy of AIM. When $\Delta p \rightarrow 0$ then all N_f dofs of the original linear system are considered and the original accuracy should be expected. Eventually, the AMG solves a linear system of equations, the solution of which is of accuracy close to Δp. At the boundaries of the decomposition, no-flow conditions are assumed. This assumption slightly modifies the initial problem in eq. (1), but for practical applications the error is low when Δp is low.

In order to update the reducing in size set N_r^{ex}, an explicit stencil is considered. Then, the least number of stable explicit time-iterations with the considered stencil is found until the explicit solution is affected by any of the implicit cells. At each iteration, cells that experienced pressure change larger than Δp are removed from the set N_r^{ex} cells and for each of them, a graph search initiates from their explicit neighboring cells and among the remaining N_r^{ex} cells. The graph updates the least number of stable time-iterations if necessary and stops searching otherwise.

3.3 Updating Seeds and Synthetic Catalogs

In a real seismic catalog, the value $M_{w,min}$ is called 'completion Magnitude' and its value depends on the seismic network. Due to the exponential nature of the Gutenberg-Richter law, the number of seismic events increases disproportionally as a better lower completion magnitude is achieved. The same disproportionate increase applies for the number of seeds that need to be sampled before every DFHM simulation since the value of $M_{w,min}$ is user-defined. In order to update the synthetic catalog of seismicity, all the sampled seeds need to be searched in every time-iteration, to interpolate pressure at their hypocenter, and to compare it with the failure

pressure. This computational cost increases disproportionally with reducing $M_{w,min}$ and efficient scalable search algorithms are required for finding where and when the criterion is satisfied.

Before the DFHM simulation, all necessary seeds are sampled as before. Then the seeds are binned to the N_r cells of the damaged matrix and the seeds within each bin are sorted with respect to their failure pressure P_f. Final step of the preprocessing, is finding for each bin the set of cells required for interpolating pressure at the bin's hypocenters. The maximum pressure value among these cells is updated with every time-iteration. Once this maximum pressure for all sets is updated, then the failure criterion is checked only for the cell's seeds with $P_f < P_{max}^k$, where P_{max}^k is the maximum value of pressure that can be needed for interpolating the pressure at the k-th damaged cell. Interpolation is still performed with a matrix-vector multiplication, but only for the seeds with $P_f < P_{max}^k$.

Henceforth, pressure is not interpolated at the hypocenters but it is considered equal to the pressure of the damaged matrix inside which they belong, and P_{max}^k is the maximum simulated pressure of the k-th cell. Without loss of generality, seeds are not allowed to reactivate twice and therefore, seeds can be triggered only when P_{max}^k change.

4. EXEMPLARY REALIZATION OF A DOUBLET STIMULATED WITH BASEL-LIKE CONDITIONS

A single realization of seeds are sampled and the scenario of a doublet is considered. The wells are vertical, parallel to each other, reach depth of 5 km, and the distance between them is 250 m. The properties of the pre-stimulated reservoir are $k_0 = 2 \cdot 10^{-17}$ m^2, $S = 1.8 \cdot 10^{-10}$ mPa^{-1} and $\rho_f = 0.4$ m^{-1}. The stimulation strategy for both wells is the step-rate injection by which the EGS well in Basel was stimulated (Fig. 1A). Injection is performed with fresh water and at a single stage, the well closes after injection, and the length of the two stimulated well segments equals the one from Basel. A coarse a-HFR model is created with grid-block size of 40 m for the damaged matrix.

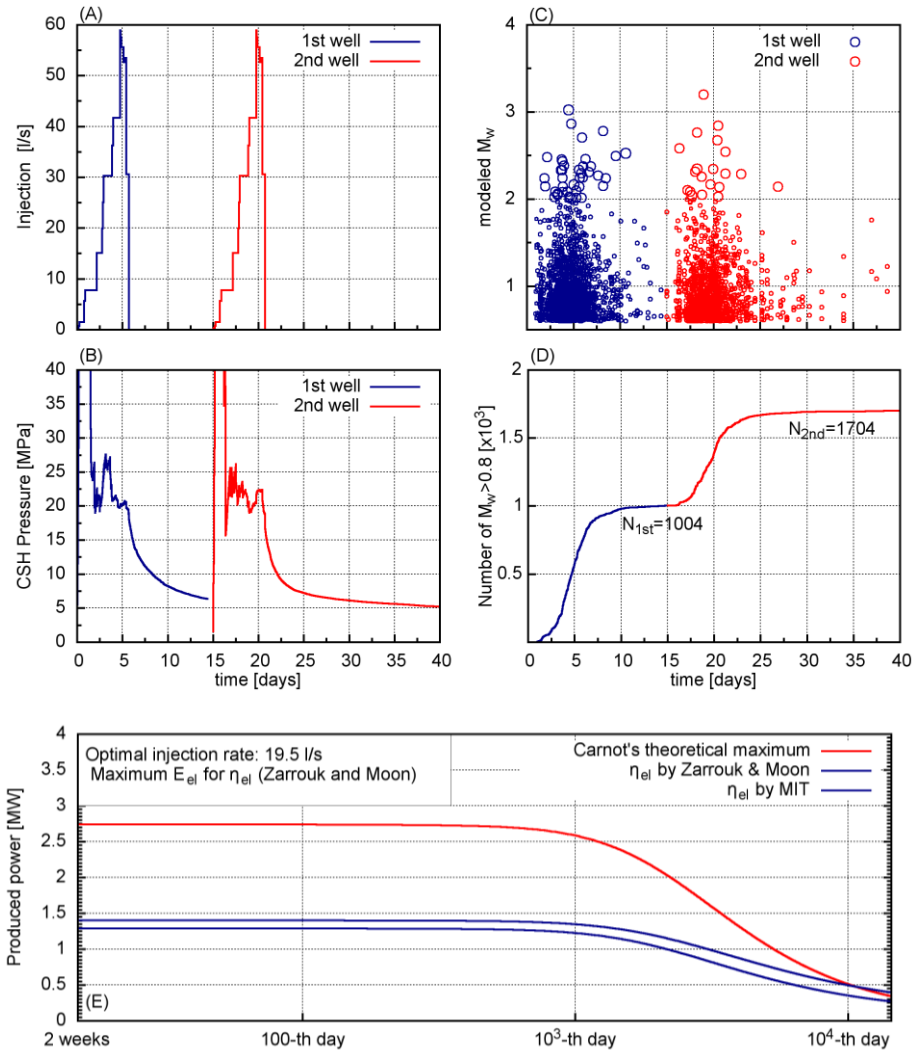

Figure 1: Simulated well logs from a single realization of slipped patches, for an EGS doublet stimulated with a strategy and with stress conditions similar to the ones in the EGS in Basel.

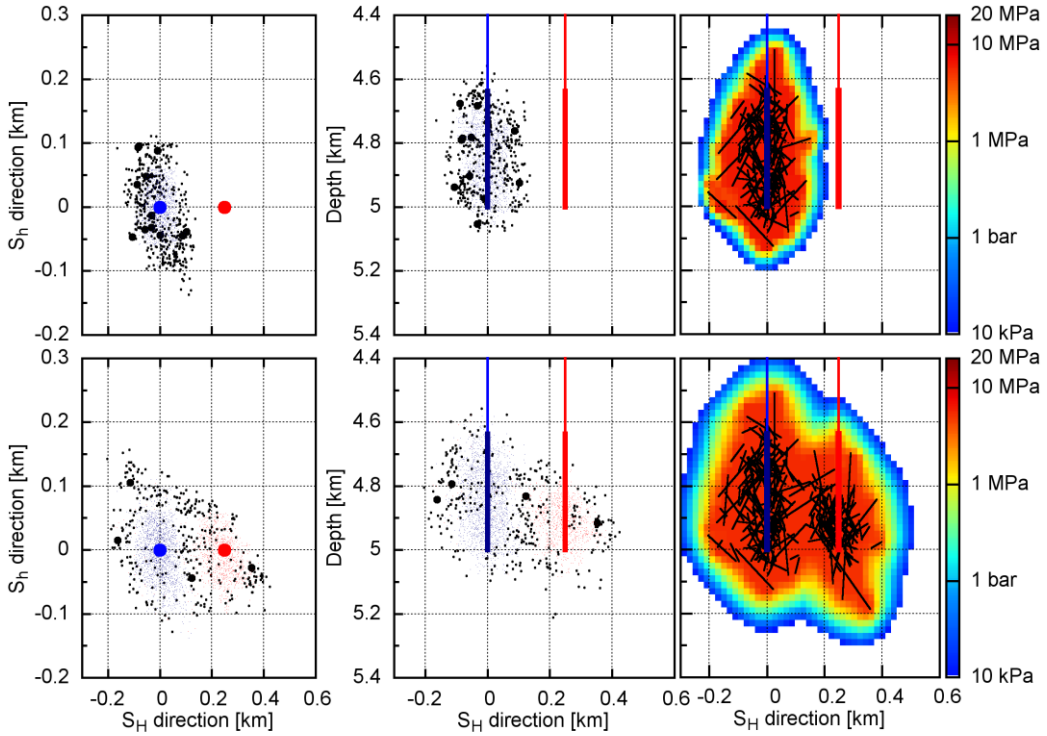

Figure 2: Snapshots of DFHM results for the 15-th and the 40-th simulated day. First two columns are the simulated hypocenters (map-view and side-view) and events with a slip patch larger than the threshold length are plotted as black circles sized according to their magnitude. The heatmap plot at the right is the simulated pressure by the a-HFR model and the traces of the slipped large patches.

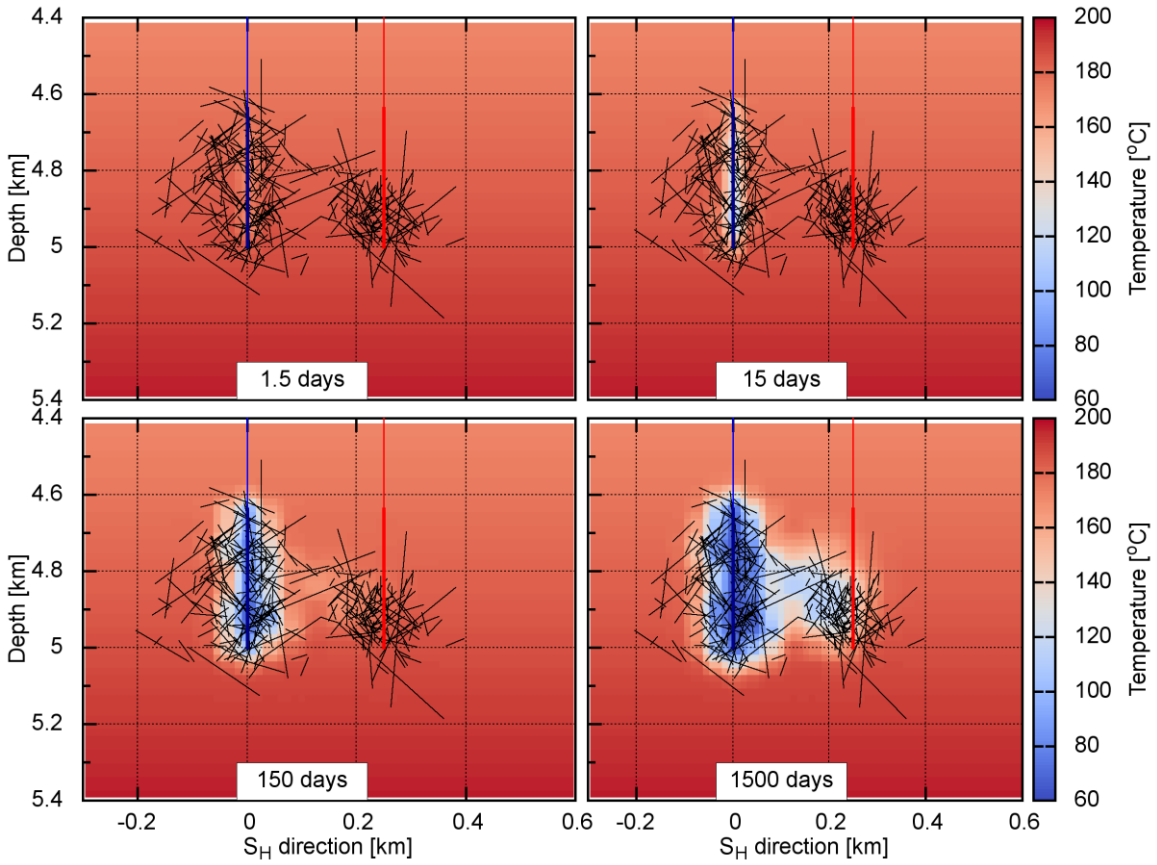

Figure 3: Snapshots of the evolution of temperature.

For the seeds fixed values are considered for $\Delta\tau$ = 2.32 MPa, μ_s = 0.6, and C_0 = 2 MPa. Two sets of seeds are sampled each with density $5 \cdot 10^{-4}$ seeds/m^2, and its magnitudes are sampled with $M_{w,min}$ = 0.6 and b-value equal to 1.3. Orientations $\boldsymbol{n}_s$ are sampled from uniform distributions for each set; it can be any orientation for the one set and at most 35° from one of the two most critical orientations. Mean stress values like in the bottom hole of the EGS in Basel (Häring et al., 2008) are assumed for all seeds, but here the maximum principal stress is assumed horizontal and aligned with the two wells and the vertical stress is the second principal stress. The three means for the principal stresses are 144 MPa, 117 MPa, and 69 MPa. The seed model assumes normally distributed stresses for the seeds with standard deviation equal to *10%* of the mean for each stress. The hydraulic aperture of slipped patches is set equal to 200 μm, and their mechanical aperture has increased from 125 μm to 1 mm.

Simulated pressure at the two casing shoes is plotted in Fig. 1B, source times and magnitudes of the simulated synthetic catalogs in Fig. 1C and the total number of simulated events with magnitude larger than 0.8 in Fig. 1D. In Fig. 2, each row has snapshots of the synthetic catalog (map-view and side-view) and a snapshot of the simulated pressure and the traces of the slipped patches with R_s larger than 20m.

Maximum possible electric revenue from the resulting network of slipped patches is found for a problem where pressure difference between the wells cannot be larger than 20 MPa, electricity cannot be generated for produced temperature below 100 °C, and the host rock is granite. The maximization is performed for the conversion efficiency of eq. (4) and it is found that a flow rate close to 19.5 l/s returns maximum electricity. This flow rate is achieved with a pressure difference at the wells 65% less than the maximum allowed. In Fig. 1E, the evolution of the generated electrical power is plotted for the efficiency considered for the optimization, the maximum efficiency of the Carnot's cycle and for the conversion efficiency suggested by Jefferson et al. (2006) and that is

$$\eta_{MIT} = 0.00052 \cdot T_p + 0.032 \,. \tag{11}$$

In Fig. 3, snapshots of the temperature evolution inside the reservoir are shown.

5. OPTIMIZING USAGE OF INDUCED SEISMICITY IN EGS DOUBLETS

Three injection strategies are studied and the one that returns maximum electricity for the least seismicity is found. Again, EGS doublets are considered and MC integration is performed with the DFHM for each strategy and for the same 250 realizations of seeds. Seeds are sampled very similarly to those of section 4, but this time the second seeds set has orientation closer to the orientation of natural fractures at the EGS in Basel. The three injection strategies have the same total injected volume per well and they are:

1. the single-stage injection q_1 that is the step-rate injection shown in Fig 1A,
2. the four-stages injection q_2, where the four stages are of equal length and the a quarter of q_1 is injected to each stage, and
3. the four-stages injection q_3 that has step-rates like q_2 but each step of q_3 lasts twice the time and is half the rate of q_2.

In Fig. 4, the forecasted probability of seismicity occurring from certain distances from the well is shown for the three strategies. The average The average number of simulated events with $M_w > 0.8$ are approximately for q_1, q_2, and q_3 approximately 1200, 700 and 550 events, respectively. Out of the 250 realizations of seeds, the strategies returned a synthetic catalog with at least one event with magnitude larger than 3.5 in 66.4%, in 78.4%, and in 84.4% of the cases.

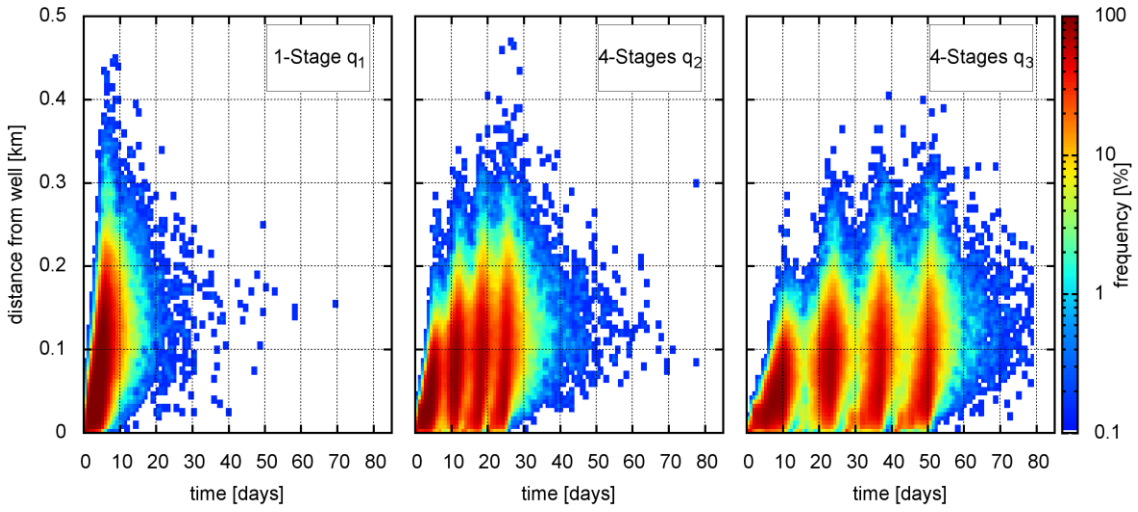

Figure 4: Distribution of the frequency with which synthetic seismicity is modeled away from the well and at any given moment.

Out of the 250 realizations of seeds, one that returned results with equally desired features for all three strategies if found. The enhanced reservoir with permeability $\boldsymbol{K}$ from each strategy is the starting point for finding the optimum distance for drilling and stimulating the second well. A Monte Carlo integration is performed for each of the 6 discrete distances, and the rate that maximizes electrical generation over a period of 25 years is found for each realization of each Monte Carlo. In Fig 5A, the expected number of events from the second well's stimulation are plotted as a function of distance and of the considered strategy. In Fig 5B, the corresponding expected maximum electrical power (averaged over 25 years) is plotted.

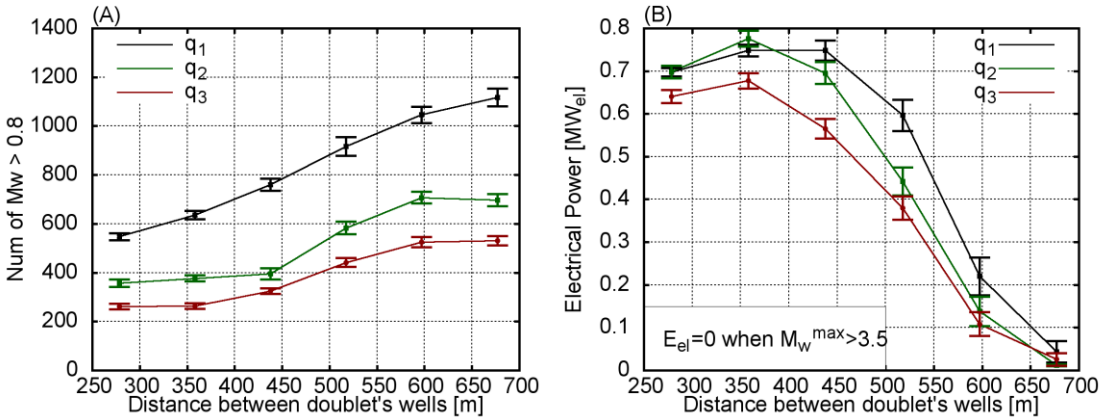

Figure 5: The expected number of events and the expected electrical power are plotted in A and B, respectively.

7. CONCLUSION

Here, it has been shown how the usage of induced seismicity in EGS can be optimized and stimulation strategies that combine low seismic hazard and maximal amounts of produced electrical energy.

Forecasts have been obtained from a three-dimensional hybrid model that employs discrete fracture modeling. The presented DFHM perform both Probabilistic Seismic Hazard Assessment and Probabilistic Reservoir Performance Assessment by simulating flow and heat transport inside dynamically changing fracture networks where injection-induced hydro-shearing occurs and permeability increases only along slipped patches.

The model is expected to assist in the development of future EGS projects in Switzerland since it is part of the ATLS developed by the Swiss Seismological Service. ATLS is a real-time risk based traffic light that integrates both all prior and real-time observations during EGS stimulations and it returns its forecasts of induced seismicity hazard and risk in time for the EGS operators to mitigate the risk. Long term forecasts of induced seismicity are possible with the DFHM. Performing PRPA in parallel with ATLS can simplify important decisions about the planned injections. Here, the assessments of the reservoir's performance are based on the expected maximum amount of electrical energy that can be generated from an EGS reservoir stimulated with a given injection plan.

Methods for accelerating forecasts of induced seismicity from the DFHM have been shown too. Besides code optimization, these methods include more efficient algorithms for managing the required huge number of sampled seeds, efficient linear system solvers for the considered EGS problems, and variations of both the adaptive step-size and the adaptive implicit method, where both of these adaptive methods allow significant acceleration of the DFHM simulation when induced seismicity is not frequent or a small reservoir volume is stimulated.

The DFHM has probabilistically compared three different stimulation strategies for a scenario similar to the EGS in Basel. The total water volume that is injected in all three strategies is the same. Compared to single stage injections with step-rate, it is shown that EGS doublets stimulated in stages are not only associated with less seismic hazard, but they can produce more electrical energy for less distanced wells and for the same amount of injected water during their stimulation.

ACKNOWLEDGEMENTS

The authors appreciate the support of Geo-Energie Suisse and of the Platform for Scientific Computing (PASC) in the development of the near real time traffic light, as well as the researchers from the Swiss National Supercomputing Center (CSCS) and from the Institute of Computational Science in USI, Lugano.

REFERENCES

Amann, F., Gischig, V., Evans, K., Doetsch, J., Jalali, R., Valley, B., Krietsch, Hannes, Dutler, Nathan, Villiger, Linus, Brixel, B., Klepikova, M., Kittilä, A., Madonna, C., Wiemer, S., Saar, M. O., Loew, S., Driesner, T., Maurer, H., Giardini, D.: The seismo-hydromechanical behavior during deep geothermal reservoir stimulations: open questions tackled in a decameter-scale in situ stimulation experiment. *Solid Earth*, **9**(1), (2018), 115–137. doi: 10.5194/se-9-115-2018

Bertani, R.: Geothermal power generation in the world 2010–2014 update report, *Geothermics*, **60**, (2016), 31–43. doi: 10.1016/j.geothermics.2015.11.003

Deb, R., & Jenny, P.: Finite volume-based modeling of flow-induced shear failure along fracture manifolds. *International Journal for Numerical and Analytical Methods in Geomechanics*, (May), (2017), 1–21. doi: 10.1002/nag.2707

Ellsworth, W. L.: Injection-Induced Earthquakes, *Science*, **341**(6142), (2013), 1225942–1225942. doi: 10.1126/science.1225942

Eshelby J. D.: The Determination of the Elastic Field of an Ellipsoidal Inclusion, and Related Problems, Proceedings of the Royal Society of London. Series A, *Mathematical and Physical Sciences* , **241**, No. 1226, (1957), pp. 376-396

Evans, K. F., Genter, A., & Sausse, J.: Permeability creation and damage due to massive fluid injections into granite at 3.5 km at Soultz: 1. Borehole observations. *Journal of Geophysical Research*, **110**(B4), (2005), B04203. doi: 10.1029/2004JB003168

Foulger, G. R., Wilson, M. P., Gluyas, J. G., Julian, B. R., & Davies, R. J. : Global review of human-induced earthquakes. *Earth-Science Reviews*, **178**, (2018), 438–514. doi: 10.1016/j.earscirev.2017.07.008

Gough, B. (2009). GNU Scientific Library Reference Manual - Third Edition (3rd ed.). Network Theory Ltd.

Grigoli, F., Cesca, S., Rinaldi, A. P., Manconi, A., López-Comino, J. A., Clinton, J. F., Westaway, R., Cauzzi, C., Dahm, T, Wiemer, S.: The November 2017 M w 5.5 Pohang earthquake: A possible case of induced seismicity in South Korea. *Science*, **360**(6392), (2018), 1003–1006. doi: 10.1126/science.aat2010

Hanks T. C., and Kanamori H.: A moment magnitude scale. *Journal of Geophysical Research*, **84**(B5), (1979), 2348. doi:10.1029/JB084iB05p02348

Häring, M. O., Schanz, U., Ladner, F., & Dyer, B. C.: Characterisation of the Basel 1 enhanced geothermal system. *Geothermics*, **37**(5), (2008), 469–495. doi: 10.1016/j.geothermics.2008.06.002

Hirschberg S, Wiemer S, Burgherr P, editors. Energy from the earth, deep geo- thermal as a resource for the future? Centre for Technology Assessment, *TA Swiss*, (2015), p. XXXI. doi: 10.3218/3655-8.

Hofmann, H., Zimmermann, G., Farkas, M., Huenges, E., Zang, A., Leonhardt, M., Kwiatek, G., Martinez-Garzon, P., Bohnhoff, M. Min, K., Fokker, P., Westaway, R., Bethmann, F., Meier, P., Yoon, K. S., Choi, J. W., Lee, T. J., Kim, K. Y.: First field application of cyclic soft stimulation at the Pohang Enhanced Geothermal System site in Korea. *Geophysical Journal International*, **217**(2), (2019), 926–949. doi: 10.1093/gji/ggz058

Karvounis, D. C., Gischig, V. S., & Wiemer, S.: Towards a Real-Time Forecast of Induced Seismicity for Enhanced Geothermal Systems. *In Shale Energy Engineering 2014* (pp. 246–255), (2014), Reston, VA: American Society of Civil Engineers. doi: 10.1061/9780784413654.026

Karvounis, D. C., & Wiemer, S.: Decision making software for forecasting induced seismicity and thermal energy revenues in enhanced geothermal systems. *Proceedings World Geothermal Congress 2015*, (April 2015), 10.

Karvounis, D. C., & Jenny, P.: Adaptive Hierarchical Fracture Model for Enhanced Geothermal Systems. *Multiscale Modeling & Simulation*, **14**(1), (2016), 207–231. doi: 10.1137/140983987

Király-Proag, E., Zechar, J. D., Gischig, V., Wiemer, S., Karvounis, D., & Doetsch, J.: Validating induced seismicity forecast models-Induced Seismicity Test Bench. *Journal of Geophysical Research: Solid Earth*, **121**(8), (2016), 6009–6029. doi: 10.1002/2016JB013236

Lee, H. S., & Cho, T. F.: Hydraulic Characteristics of Rough Fractures in Linear Flow under Normal and Shear Load. *Rock Mechanics and Rock Engineering*, **35**(4), (2002), 299–318. doi: 10.1007/s00603-002-0028-y

Lee, K.-K., Ellsworth, W. L., Giardini, D., Townend, J., Ge, S., Shimamoto, T., … Langenbruch, C: Managing injection-induced seismic risks. *Science*, **364**(6442), (2019), 730–732. doi: 10.1126/science.aax1878

Lu, S.-M.: A global review of enhanced geothermal system (EGS). *Renewable and Sustainable Energy Reviews*, **81**, (2018), 2902–2921. doi: 10.1016/j.rser.2017.06.097

Malin, P., Kwiatek, G., Saarno, T., & Dresen, G.: Controlling Seismicity During a 6.1-km-Deep Geothermal Stimulation in Finland. Acta Geologica Sinica - English Edition, **93**(S1), (2019), 190–191. doi: 10.1111/1755-6724.14030

Mignan, A., Broccardo, M., Wiemer, S., & Giardini, D.: Induced seismicity closed-form traffic light system for actuarial decision-making during deep fluid injections. *Scientific reports*, **7**(1), (2017), 13607. doi: 10.1038/s41598-017-13585-9

MIT. The future of geothermal energy, impact of enhanced geothermal systems (EGS) on the United States in the 21st Century, Massachusetts Institute of Technology, 2006, ISBN: 0-615-13438-6.

Mourzenko, V., Thovert, J.-F., & Adler, P.: Percolation of three-dimensional fracture networks with power-law size distribution. *Physical Review E*, **72**(3), (2005), 036103. doi: 10.1103/PhysRevE.72.036103

Peaceman, D. W.: Interpretation of Well-Block Pressures in Numerical Reservoir Simulation, *Society of Petroleum Engineers Journal*, **18**(3), (1978), 183–194. doi: 10.2118/6893-PA

Thomas, G. W., & Thurnau, D. H.: Reservoir Simulation Using an Adaptive Implicit Method, *Society of Petroleum Engineers Journal*, **23**(05), (1983), 759–768. doi: 10.2118/10120-PA

van der Elst, N. J., Page, M. T., Weiser, D. A., Goebel, T. H. W., & Hosseini, S. M.: Induced earthquake magnitudes are as large as (statistically) expected. *Journal of Geophysical Research: Solid Earth*, **121**(6), (2016), 4575–4590. doi: 10.1002/2016JB012818

van Thienen-Visser, K., & Breunese, J. N.: Induced seismicity of the Groningen gas field: History and recent developments, *The Leading Edge*, **34**(6), (2015), 664–671. doi: 10.1190/tle34060664.1

White, J. A., & Foxall, W.: Assessing induced seismicity risk at CO2 storage projects: Recent progress and remaining challenges. *International Journal of Greenhouse Gas Control*, **49**, (2016), 413–424. doi: 10.1016/j.ijggc.2016.03.021

Zarrouk, S. J., & Moon, H.: Efficiency of geothermal power plants: A worldwide review. *Geothermics*, **51**, (2014), 142–153, doi: 10.1016/j.geothermics.2013.11.001